Transient anomaly in fault-zone trapped waves during the preparatory phase of the 6 April 2009, Mw 6.3 L'Aquila earthquake

Giovanna Calderoni, Antonio Rovelli, and Rita Di Giovambattista
Istituto Nazionale di Geofisica e Vulcanologia
Via di Vigna Murata 605
00143 Rome, Italy

Abstract

Fault-zone trapped waves generated by repeating earthquakes of the 2009 L'Aquila seismic sequence show a sudden, up to 100% increase of spectral amplitudes seven days before the mainshock. The jump occurs ten to twenty hours after the M_L 4.1, 30 March 2009 largest foreshock. The amplitude increase is accompanied by a loss of waveform coherence in the fault-trapped wavetrain. Other geophysical and seismological parameters are known to have shown a sudden change after the 30 March foreshock. The concomitance of a consistent change in the fault-zone trapped waves leads us to interpret our observation as due to a sudden temporal variation of the velocity contrast between the fault damage zone and hosting rocks in the focal volume. Fault-zone trapped waves thus provide a refined time resolution for changes occurring near the rupture nucleation, with the indication of a strong variation in one day.

1) Introduction

The Mw 6.3, 6 April 2009 L'Aquila earthquake was preceded by a long suite of foreshocks, the largest one (M_L 4.1) occurred on 30 March at 13:38 (UTC). This event marked the beginning of an abrupt temporal change in different seismic parameters such as the b-value [*Papadopoulos et al*., 2010; *Sugan et al*., 2014], the spatio-temporal distribution of the events [*Telesca*, 2010], the P-to-S wave velocity ratio [*Di Luccio et al*., 2010; *Lucente et al*., 2010]. Using a cross-correlation analysis of ambient noise, *Zaccarelli et al*. [2011] observed a drop of 0.3% in crustal velocity that was associated to a perturbation of elastic properties in the L'Aquila region.

Foreshocks before and after the M_L 4.1 foreshock have different locations, frequency and magnitude distribution (Fig. 1). Before that event, seismicity was concentrated to the North of the volume where the main shock nucleated. After the M_L 4.1 event, rate and magnitude of foreshocks increased and seismicity migrated toward the main shock nucleation zone. These features of seismicity make difficult to assess precisely to what extent the changes in seismic parameters found in some of the above-mentioned papers are in time or in space. As remarked by *Savage* [2010], this ambiguity is not completely solved when only a small group of foreshocks has similar location of aftershocks. In this study, we base our inferences on waveforms of repeating earthquakes. These events occurred in the crustal volume where the Mw 6.3 main shock nucleated, and their waveforms are used to discriminate spatial from temporal variations of elastic parameters along the fault. We analyze amplitudes of fault-zone trapped waves (FZTWs) recorded at FAGN, a broad-band station of the permanent network run by Istituto Nazionale di Geofisica e Vulcanologia (INGV). This station is aligned along the strike of the main fault, about 20 km to the southeast of the main shock epicenter.

Amplitude variations in FZTWs have been object of previous studies [*Calderoni et al*., 2010, 2012] where two clusters were found to promote the most efficient FZTWs at FAGN. These clusters are located in the northwestern and southeastern tips of the fault plane of the main shock rupture, as

46 shown by the color scale in the inset of Fig. 1. The question addressed here is whether the
47 amplitude variations of FZTWs as found by *Calderoni et al*. [2012] have a spatial origin only or do
48 they imply temporal variations as well. The events of the northwestern cluster are particularly well
49 suited to face the issue as they sample a part of the main shock preparation volume throughout a
50 long time interval including both foreshocks and aftershocks. Differences in their waveforms thus
51 reflect changes in elastic properties along the ray-path [see also *Poupinet et al.,* 1984; *Ellsworth et*
52 *al.,* 1992; *Schaff and Beroza*, 2004].
53
54 **2) Search for repeating earthquakes**
55 Waveforms of repeating earthquakes are selected among seismograms recorded by three 24-bits
56 broad band seismological stations (namely AQU, FAGN and FIAM) operated by INGV in the
57 epicentral area (Fig. 1). Seismograms are available on line at http://iside.rm.ingv.it.
58 The northwestern cluster as originally identified by *Calderoni et al*. [2012] was composed of 19
59 events (see the inset of Fig. 1). After a new search in the database, eighteen more events with
60 similar hypocenter determinations were found. For a preliminary selection we checked both
61 hypocenter determinations of the INGV bulletin (at http://bollettinosismico.rm.ingv.it/) and those
62 by *Chiaraluce et al*. [2011] that used a more refined double-difference (DD) algorithm [*Waldhauser*
63 *and Ellsworth*, 2000]. Therefore, the waveform similarity of earthquakes was estimated with a
64 cross-correlation analysis in the time domain following the procedure of *Console and Di*
65 *Giovambattista* [1987]. We analyzed seismograms of FIAM as the ray path from the cluster to this
66 station crosses the rupture volume to a minor extent. As discussed by *Di Luccio et al*. [2010], FIAM
67 and FAGN have comparable distance from the nucleation volume but ray paths of FIAM, which are
68 transversal to the fault, are less sensitive to local spatial variations compared to FAGN where ray
69 paths go along strike.
70 To estimate the coherence of waveforms of FIAM, the cross-correlation coefficient (CC) was
71 computed using the vertical and fault-parallel components after band-pass filtering between 1 and 6

Hz. We extracted a 4-s time window starting with the P-wave onset and including the arrivals of the direct S-wave. The largest S-wave pulse dominates the cross-correlation minimizing the influence of the background noise. In the procedure for the computation of CC, the first sample of the time window starts 0.1 s before the manually picked P arrival time, then samples are shifted with a 1 sample increment. Each of the analyzed waveforms of FIAM is correlated against all of those recorded at the same station, and the resulting values of CC are stored in a cross-correlation matrix. This matrix is used to identify a master event showing the highest similarity among events (earthquake # 5 in Table 1) and select repeaters. Vertical and fault-parallel components lead to the same conclusions, results from the fault-parallel component are used hereinafter. At the end of a comparative check, 15 events with $M_L > 2$ resulted in the range $0.8 \leq CC \leq 0.96$, and 2 events in the range $0.7 \leq CC < 0.8$. The other events were not considered in the analysis. Waveforms of FIAM for these selected events are plotted in Figure 2 (column to the left and in the middle), superimposed to the master event.

When the seismograms of the other two stations AQU and FAGN are considered, we note that event # 5, identified as master event with waveforms of FIAM, was not recorded by FAGN and three events (# 6, 7, and 8) available at FAGN were not recorded by FIAM (see Table 1). To check if the latter three events have an acceptable correlation degree, we cross-correlated the seismograms of FAGN with another event (#4) recorded by FAGN and having a very high correlation at FIAM. The resulting cross-correlation coefficients obtained for waveforms of FAGN in the two groups (simultaneously available and not available at FIAM) were generally smaller than those of FIAM, as expected, but are comparable for the two groups. Therefore, the three events recorded at FAGN were accepted for the next analyses, they are included in Table 1 and plotted in Figure 2 (column to the right).

3) Study of the transient change

Waveforms of the 20 repeaters selected in the previous section are used to seek for temporal variations in the fault-zone properties in a time interval spanning from February 2009 to July 2010. As already observed by *Calderoni et al*. [2010, 2012], FZTWs recorded at FAGN cause systematic larger amplitudes in post-S wavetrains compared to the other two stations. This relative increase of ground motion has been interpreted and modeled as the resonant fundamental mode of the fault-zone excitation that affects mostly the frequency band 1-3 Hz. To investigate temporal variations in the repeater sequence, in this paper we first use the same parameter already adopted by *Calderoni et al*. [2012], i.e. the spectral ratio in the frequency band 1–3 Hz between FAGN and AQU. The time window used by *Calderoni et al*. [2012] was 10 s long bracketing direct S-waves and post-S largest amplitudes phases of the fault-parallel component. In seismograms of FAGN, this time window is dominated by FZTWs [*Calderoni et al.,* 2010]. Fig. 3a depicts the trend of the geometric mean, in the frequency band 1 – 3 Hz, of the FAGN/AQU spectral ratios for repeating earthquakes available both at FAGN and AQU. Error bars indicate a 95% confidence interval. We can see a statistically significant, sharp increase in one day (30 March 2009). This jump is of the order of 100% compared to the level of amplitude of previous foreshocks.

For the sake of comparison, the time variation of seismic velocity in the preparatory volume of the Mw 6.3 main shock [as found by *Zaccarelli et al*., 2011] is also plotted with the same temporal axis (Fig. 3b). A co-seismic velocity decrease was also observed at the San Andreas Fault immediately after the 2004 M6 Parkfield earthquake [*Li et al*., 2006, 2007]. Although the time resolution of the analysis by *Zaccarelli et al*. [2011] is much lower because of the 50 days stacking length needed in their analysis, we note a consistent trend in the two plots of Figs. 3a and 3b in coincidence with the main shock preparatory phase. According to *Di Luccio et al*. [2010] a sharp change in the seismicity rate is observed after the M_L 4.1 foreshock of 30 March 2009 (Fig. 3c). The amplitude variation of

121 FZTWs also starts immediately after the strongest foreshock. Note that the M_L 4.1 foreshock is one
122 (# 4) of the repeating earthquakes of our cluster.
123 In principle, spectral ratios of Fig. 3a are controlled by both numerator (FAGN) and denumerator
124 (AQU) spectra, then their contribution to the ratio is undetermined a priori. Further investigations
125 are needed to check their relative weight and isolate the role of ray paths to FAGN in the sudden
126 temporal change. A new evidence that the propagation in the fault-zone had a major role is provided
127 by the loss of waveform coherency in the FZTWs recorded at FAGN. According to *Taira et al.*
128 [2008, 2009], the decorrelation index (defined as 1 – CC) is the optimal parameter to represent the
129 loss of waveform coherency. Fig. 3a depicts time variations of the coherence reduction in repeaters
130 of FAGN when CC is computed in a 4 s time window beginning with the direct S wave and
131 including early trapped waves. For the sake of comparison, the amplitude of spectral ratios
132 FAGN/AQU and the decorrelation index are plotted together. In Fig. 3 a there is an impressive
133 match between these two completely independent parameters: the sudden jump in decorrelation
134 starts in the repeaters immediately after the M_L 4.1 foreshock reproducing the same onset of the
135 FAGN/AQU spectral ratio. The two trends go similarly high until the main shock rupture then they
136 gradually decrease. A similar drop of coherence was observed in concomitance with the 1999, Mw
137 7.1 Duzce earthquake in the Northern Anatolian Fault [*Roux and Ben-Zion*, 2014], with a well
138 constrained transient duration of four days in their study. Unfortunately, the L'Aquila seismic
139 sequence was characterized by a strong seismicity migration from the nucleation volume after the 6
140 April main shock [*Di Luccio et al*., 2010]. This caused a significant depletion of repeaters in the
141 nucleation volume and the small number of repeaters after the main shock in our cluster does not
142 allow to constrain the gradual recovery with the same dense sampling as in the onset. However, Fig.
143 3a shows that late repeaters of June 2009 go down to an amplitude level comparable to the one of
144 early foreshocks, as also indicated (see Fig. 4) by the strong waveform similarity of event # 2 with
145 event # 14 of 20 June, the former representing the situation before the jump of 30 March. In Fig.4

146 the waveforms in the upper panels (c, d and e) are relative to events occurred between 30 March
147 and 6 April while in the bottom panels events with background amplitudes are shown. The strong
148 temporal variation of waveforms in panels c to e consists in both an amplitude increase and a phase
149 change in the post-S waves. The variation in post-S wavetrains is then further quantified using the
150 spectral ratio between FZTW and direct S-waves of each event. According to the spectrograms of
151 *Calderoni et al* [2010], the wavetrain of FZTWs coming from the cluster beneath AQU begins 1.5
152 to 2 s after the direct S waves. We extracted a time window of 1.5 s of S waves and a time window
153 of 4.5 s including FZTWs, both starting with the first S arrival. The spectral ratios between these
154 wavetrains for each event are shown in Fig. 4 (red symbols in the central panel). Due to the stability
155 of the direct S waveforms of repeaters, the FZTW/S spectral ratio is a valid indicator of the
156 temporal change of the impedance contrast between the hosting rock and the fault damage zone.
157 This is a much more direct indicator of the fault-zone behavior than FAGN/AQU spectral ratio
158 where also variations in the ray-paths to AQU could have had a role. The FZTW/S spectral ratios
159 confirm a factor of 2 variation in the amplitude jump.
160

161 ## 4) Discussion

162 The increase in amplitudes of FZTWs of co-located repeating earthquakes after the 30 March
163 largest foreshock can be interpreted in terms of a temporal change in the fault-zone properties or a
164 different coupling between the causative earthquakes and the fault zone. *Peng and Ben-Zion* [2006]
165 used the evolving phase delays of cross-correlations of repeating events waveforms to estimate the
166 time delay and then the percentage of velocity change in the Karadere-Duzce Branch of the North
167 Anatolian Fault. *Wu et al*. [2009] used the solution of *Ben-Zion and Aki* [1990] to convert changes
168 in spectral results to percent change of velocities.
169 According to *Fohrmann et al*. [2004] and *Li and Vidale* [2006] the generation of FZTW is very
170 sensitive to small variations of the position of causative earthquakes close the fault zone. Based on

171 the predominant frequency (≈5 Hz) in seismograms of FIAM, the λ/4 criterion [*Geller and Mueller*,
172 1980] suggests that good waveform correlation can exist when separation between repeaters is not
173 greater than two hundred meters. In principle, the upper limit of this inter-event distance is large
174 enough to cause a different excitation of the fault zone. However, events that show a decrease of
175 coherence in the FZTWs of FAGN are characterized by an increase of coherence in the
176 seismograms of FIAM (see Fig. 2), and this opposite behavior suggests that separation between
177 repeaters after the 30 March largest foreshock is not larger than the one of early foreshocks.
178 Moreover, the fault plane solution of event # 4 [*Herrmann et al*., 2011] indicates normal
179 mechanisms with ruptures in the fault plane for all the events of the cluster. Therefore, the possible
180 up to ≈ 200 m separation between repeaters likely occurs parallel to the fault plane, and this
181 condition guarantees that a different coupling can have only a secondary role in our observations.
182 The concomitant evidence of other temporal changes in seismological [*Telesca*, 2010; *Papadopulos*
183 *et al*., 2010; *Sugan et al*., 2014] and geophysical parameters [*Di Luccio et al*., 2010; *Lucente et al*.,
184 2010] after the M_L 4.1 foreshock leads us to ascribe the observed effect primarily to a velocity
185 change in the damage fault zone.
186 The sharp onset of spectral ratios and decorrelation index at FAGN (Fig. 3 and 4) is thus used as a
187 time marker for a sudden increase of the seismic impedance contrast between the damage fault zone
188 and the hosting rock. The crack growth within the rupture zone could be the main cause of the
189 velocity decrease. Several authors [*Di Luccio et al*., 2010; *Lucente et al*., 2010] invoked a role of
190 fluid migration in the preparatory volume of the rupture. This effect can also explain the increase
191 in Vp/Vs observed in the region. As discussed in *Di Luccio et al*. [2010], models of fluid migration
192 [e.g. *Zhang and Sanderson*, 1996] predict that the permeability of the fault increased along the
193 direction of the maximum horizontal stress and fluid flow was thus favored along the fault strike. In
194 central Apennines the evidence of pressurized, mantle-derived fluids is given by the high CO_2
195 release ($1–5 \times 10^6$ mol km^{-2} yr^{-1}) [*Chiodini et al*., 2000]. The role of fluids was also confirmed by

196 geochemical surveys in two regional aquifers located in the epicentral area [*Chiodini et al*., 2011].
197 Evidence of the presence of fluids in the seismogenic volume where the analyzed cluster occurs is
198 discussed in *Calderoni et al*. [2012] based on previous results of *Terakawa et al*. [2010].
199 In this framework, the time variations observed in this study could be related to variations of fluid
200 pressure in the ruptured fault zone that could be responsible for the significant decrease of shear-
201 wave velocity. Compared to the size of the anomalies observed for Vp/Vs (of the order of few
202 percent), our observations suggest that the variation of shear waves in the fault zone was probably
203 much larger. As a matter of fact, the fault zone impedance contrast could have attained a 100%
204 variation, but this represents an upper limit that is valid only for a zero-variation of the source
205 coupling of causative earthquakes with the fault.
206

207 ## 5) Conclusions

208 In this work we describe temporal changes occurred in the fault zone seven days before the
209 L'Aquila main shock. The transient is well constrained through the waveforms of co-located
210 repeaters before and after the mainshock. Three independent techniques show that

211 i. The level of fault excitation estimated as a spectral ratio between on-fault (FAGN)
212 and off-fault (AQU) receivers increased suddenly immediately after the 30 March,
213 M_L 4.1 foreshock. This increase persists until the occurrence of the mainshock and
214 then gradually decreases.
215 ii. The temporal trend of waveform coherency of FZTWs recorded at FAGN mimics
216 the amplitude transient. The decorrelation index (1-CC) shows a significantly similar
217 jump after the M_L 4.1 foreshock as observed in the FAGN/AQU spectral ratio.
218 iii. Direct S waves of repeaters maintain a stable shape while the FZTW wavetrain loses
219 its coherence for tens of days after the largest foreshock. The spectral ratio between
220 FZTWs and direct S waves of FAGN yields consistent amplitude variations
221 compared to (i).

222 Therefore, independent parameters provide the same time signature, indicating the M_L 4.1
223 foreshock as a marker for the onset of the temporal variations. Changes in the FZTWs of FAGN are

likely dominated by the variation of the impedance contrast between the hosting rock and the fault damage zone. Spectral ratios yield a factor of 2 amplitude variation thus suggesting that the change of shear-wave velocity in the fault zone could be very large locally, depending on physical processes occurring during the preparatory phase. These include the flow of fluids within the damage zone or the opening and growth of cracks. The shortcoming of this study is the inability to precisely assess the velocity variation in the fault zone due to the impossibility of separating the two competing effects of the velocity change and the varying source coupling of causative earthquakes with the fault for possible, although small, hypocenter variations transversally to the fault plane.

Acknowledgments

Some of the figures were done using GMT [*Wessel and Smith*, 1991]. The Seismic Analysis Code (SAC) [*Goldstein et al*., 2002] was used for much of the analysis.
The broad band data using in this paper were recorded by seismological stations of the Italian Seismic Network run by Istituto Nazionale di Geofisica e Vulcanologia (INGV).These waveforms are available at http://iside.rm.ingv.it.
We thank the Editor Andrew W. Newman, Yong Gang Li and an anonymous reviewer for many useful and constructive critical comments. Discussions with Guido Ventura were very helpful in the development of this research.

References

Ben-Zion, Y., and K. Aki (1990), Seismic radiation from an SH line source in a laterally heterogeneous planar fault zone, *Bull. Seism. Soc. Am*., 80, 971-994.

Calderoni, G., A. Rovelli, and R. Di Giovambattista (2010), Large amplitude variations recorded by an on-fault seismological station during the L'Aquila earthquakes: Evidence for a complex fault-induced site effect, *Geophys. Res. Lett*., 37, L24305, doi:10.1029/2010GL045697.

Calderoni, G., R. Di Giovambattista, P. Vannoli, S. Pucillo, and A. Rovelli (2012), Fault-trapped waves depict continuity of the fault system responsible for the 6 April 2009 Mw 6.3 L'Aquila earthquake, central Italy, *Earth Planet. Sci. Lett*., 323, 1–8, doi:10.1016/j.epsl.2012.01.003.

Chiaraluce, L., L. Valoroso, D. Piccinini, R. Di Stefano, and P. De Gori (2011), The anatomy of the 2009 L'Aquila normal fault system (central Italy) imaged by high resolution foreshock and aftershock locations, *J. Geophys. Res*., 116, B12311, doi:10.1029/2011JB008352.

Chiodini, G., F. Frondini, C. Cardellini, F. Parello, and L. Peruzzi (2000), Rate of diffuse carbon dioxide Earth degassing estimated from carbon balance of regional aquifers: The case of central Apennine, Italy, *J. Geophys. Res*., 105(B4), 8423–8434, doi:10.1029/1999JB900355.

Chiodini, G., A. Caliro, C. Cardellini, F. Frondini, S. Inguaggiato and F. Matteucci (2011), Geochemical evidence for and characterization of CO2-rich gas sources in the epicentral area of the Abruzzo 2009 earthquakes, *Earth Planet. Sci. Lett*., 304, 389–398, doi:10.1016/j.epsl.2011.02.016.

Console, R. and R. Di Giovambattista (1987), Local earthquake relative location by digital records, *Phys. Earth Planet. Inter*., 47, 43–49, doi:10.1016/0031-9201(87)90065-3.

Di Luccio, F., G. Ventura, R. Di Giovambattista, A. Piscini, and F. R. Cinti (2010), Normal faults and thrusts reactivated by deep fluids: The 6 April 2009 Mw 6.3 L'Aquila earthquake, central Italy, *J. Geophys. Res*., *115*, B06315, doi:10.1029/2009JB007190.

DISS Working Group (2010). Database of Individual Seismogenic Sources (DISS), Version 3.1.0: A compilation of potential sources for earthquakes larger than M 5.5 in Italy and surrounding areas. http://diss.rm.ingv.it/diss/, © INGV 2009.

Ellsworth, W. L., A. T. Cole, G. C. Beorza, and M. C. Verwoerd (1992), Changes in crustal wave velocity associated with the 1989 Loma Prieta, California, earthquake, Eos Trans. AGU, 73(43), Fall Meet. Suppl., F360.

Falcucci, E., S. Gori, E. Peronace, G. Fubelli, M. Moro, M. Saroli, B. Giaccio, P. Messina, G. Naso, G. Scardia, A. Sposato, M. Voltaggio, P. Galli, and F. Galadini (2009), The Paganica fault and surface coseismic ruptures due to the April 6, 2009 earthquake (L'Aquila, Central Italy), *Seismol. Res. Lett*. 80, 6, doi:10.1785/gssrl.80.6.940.

Fohrmann, M., H. Igel, G. Jahnke, and Y. Ben-Zion (2004), Guided waves from sources outside faults: an indication for shallow fault zone structure? *Pure Appl. Geophys*., 161, 2125–2137, doi:10.1007/s00024-004-2553-y.

Galli, P., B. Giaccio, and P. Messina (2010), The 2009 central Italy earthquake seen through 0.5 Myr-long tectonic history of the L'Aquila faults system, *Quat. Sci. Rev.* 29, 3768–3789, doi:10.1016/j.quascirev.2010.08.018.

Geller, R, and C. Mueller (1980), Four similar earthquakes in central California, *Geophys. Res. Lett*., 7, 821-824, doi:10.1029/GL007i010p00821.

Goldstein, P., D. Dodge, M. Firpo, and L. Minner (2003), SAC2000: Signal processing and analysis tools for seismologists and engineers. *International Handbook of Earthquake and Engineering Seismology*, W. H. K. Lee, H. Kanamori, P. C. Jennings, and C. Kisslinger Editors, chapter 85.5 San Diego: Academic Press.

Herrmann, R.B., L. Malagnini, and I. Munafò (2011), Regional moment tensors of the 2009 L'Aquila earthquake sequence, *Bull. Seismol. Soc. Am.* 101, doi: 10.1785/0120100184.

Li, Y. G., and J. E. Vidale (1996). Low-velocity fault zone guided waves: Numerical investigations of trapping efficiency, *Bull. Seism. Soc. Am*., 86, 371-378, 1996.

Li, Y. G., P. Chen, E. S. Cochran, J. E., Vidale, and T. Burdette (2006), Seismic evidence for rock damage and healing on the San Andreas fault associated with the 2004 M6 Parkfield earthquake, *Bull. Seism. Soc. Am*., 96(4), S1-S15, doi:10.1785/0120050803,

Li, Y. G., P. Chen, E. S. Cochran, and J. E. Vidale (2007), Seismic velocity variations on the San Andreas Fault caused by the 2004 M6 Parkfield earthquake and their implications, *Earth Planets Space*, 59, 21-31.

Lucente, F. P., P. De Gori, L. Margheriti, D. Piccinini, M. Di Bona, C. Chiarabba, and N. Piana Agostinetti (2010), Temporal variation of seismic velocity and anisotropy before the 2009 Mw 6.3 L'Aquila earthquake, Italy, *Geology*, 38, 1015–1018, doi:10.1130/G31463.1.

Papadopoulos, G.A., M. Charalampakis,A. Fokaefs, and G. Minadakis (2010), Strong foreshock signal preceding the L'Aquila (Italy) earthquake (Mw 6.3) of 6 April 2009, *Nat. Hazards Earth Syst. Sci*. 10 (1), 19–24, doi:10.5194/nhess-10-19-2010.

Peng, Z., and Y. Ben-Zion (2006), Temporal changes of shallow seismic velocity around the Karadere-Duzce Branch of the North Anatolian Fault and strong ground motion, *Pure Appl. Geophys*., 163 (2006) 567–600, doi: 10.1007/s00024-005-0034-6.

Poupinet, G., W. L. Ellsworth, and J. Frechet (1984), Monitoring velocity variations in the crust using earthquake doublets: An application to the Calaveras fault,California, *J. Geophys. Res*., 89, 5719-5731, 1984, doi:10.1029/JB089iB07p05719.

Roux, P., and Y. Ben-Zion (2014), Monitoring fault zone environments with correlations of earthquake waveforms, *Geophys. J. Int*., 196, 1073–1081, doi:10.1093/gji/ggt441.

Savage, M. K. (2010), The role of fuids in earthquake in the 2009 Mw 6.3 L'Aquila, Italy, earthquake and its foreshocks, *Geology* 38, 1055–1056, doi: 10.1130/focus112010.1

Schaff, D. P., and G. C. Beroza (2004), Coseismic and postseismic velocity changes measured by repeating earthquakes, *J. Geophys. Res*., 109, B10302, doi:10.1029/2004JB003011.

Sugan, M., A. Kato, H. Miyake, S. Nakagawa, and A. Vuan (2014), The preparatory phase of the 2009Mw 6.3 L'Aquila earthquake by improving the detection capability of low-magnitude foreshocks, *Geophys. Res. Lett*., 41, doi:10.1002/2014GL061199.

Taira, T., P. G. Silver, F. Niu, and R. M. Nadeau (2008), Detecting seismogenic stress evolution and constraining fault zone rheology in the San Andreas Fault following the 2004 Parkfield earthquake, *J. Geophys. Res*., 113, B03303, doi: 10.1029/2007JB005151.

Taira, T., P. G. Silver, F. Niu and R. M. Nadeau (2009), Seismic evidence for remote triggering of fault-strength changes on the San Andreas fault at Parkfield, *Nature*, 461, 636–640, doi:10.1038/nature08395.

Telesca, L. (2010), A non-extensive approach in investigating the seismicity of L'Aquila area (central Italy), struck by the 6 April 2009 earthquake (M_L = 5.8), *Terra Nova*, 22, 87–93, 2010b, doi:10.1111/j.1365-3121.2009.00920.x

Terakawa, T., A. Zoporowski, B. Galvan, and S.A. Miller (2010), High-pressure fluid at hypocentral depths in the L'Aquila region inferred from earthquake focal mechanisms, *Geology,* 38, 995–998, doi:10.1130/G31457.1.

Vezzani, L., and F. Ghisetti (1998), Carta geologica dell'Abruzzo, Scala 1:100.000, S.El.Ca., Florence, Italy.

Waldhauser, F., and W. L. Ellsworth (2000), A double-difference earthquake location algorithm: method and application to the northern Hayward Fault, *Bull. Seismol. Soc. Am*., 90, 1330-1368, doi: 10.1785/0120000006.

Wessel, P., and W. H. F. Smith (1991), Free software helps map and display data, *Eos Trans. AGU*, 72, 441, doi: 10.1029/90EO00319.

Wu, C., Z. Peng, and Y. Ben-Zion (2009), Non-linearity and temporal changes of fault zone site response associated with strong ground motion, *Geophys. J. Int*., 176, 265–278, doi: 10.1111/j.1365-246X.2008.04005.x.

Zaccarelli, L., N. M. Shapiro, L. Faenza, G. Soldati, and A. Michelini (2011), Variations of crustal elastic properties during the 2009 L'Aquila earthquake inferred from cross-correlations of ambient seismic noise, *Geophys. Res. Lett*., 38, L24304, doi: 10.1029/2011GL049750.

Zhang, X., and D. J. Sanderson (1996), Effects of stress on the two dimensional permeability tensor of natural fracture networks, *Geophys. J. Int*., 125, 912–924, doi:10.1111/j.1365-246X.1996.tb06034.x.

Table Captions

Table 1: Source parameters of repeating earthquakes used in this study.

Figure Captions

Figure 1: Map of the study area with epicenters of the 2009 L'Aquila seismic sequence. Black triangles are the broad-band seismological stations AQU, FAGN, and FIAM used in this paper. The orange rectangle is the projection onto the surface of the ruptured fault plane of the 6 April 2009, Mw 6.3 earthquake [the Paganica Seismogenic Source of *DISS Working Group*, 2010], and the white star indicates the rupture nucleation patch. Gray symbols are aftershocks, and green and bleu symbols are foreshocks before and after the M_L 4.1, 30 March foreshock, respectively. Red lines represent active faults in the region according to *Vezzani and Ghisetti* [1998], *Falcucci et al.* [2009] and *Galli et al.* [2010]. In the inset, colored dots represent epicenters of causative earthquakes that

401 generated FZTWs at FAGN, the color scale quantifies their relative (log) amplification in the
402 frequency band 1 – 3 Hz [after *Calderoni et al*., 2012].
403
404 **Figure 2:** Waveforms of repeating earthquakes (in red) superimposed to the master event (in black).
405 The largest part of them was selected using station FIAM, in a position substantially orthogonal to
406 the fault strike (master event # 5). Three events were not recorded by FIAM and seismograms of the
407 on-fault station FAGN were used (master event # 4). Waveforms of this station show a larger
408 complexity due to the effect of the propagation in the fault and result in generally lower CC than
409 those of FIAM when both are available. The fault plane solution of the M_L 4.1, 30 March largest
410 foreshock is redrawn from *Herrmann et al*. [2011]. It is representative of focal mechanism of the
411 entire cluster.
412
413 **Figure 3:** (a) Amplitude variations of FZTWs (in black) as inferred from the FAGN/AQU spectral
414 ratios using the horizontal fault-parallel components. Error bars indicate 95% of the confidence
415 interval in the 1-3 Hz frequency band. Red symbols are decorrelation values (1-CC) of the FAGN
416 waveforms using a 4-s time window bracketing FZTWs. The zooming image in the inset shows to
417 what extent the match is strict between these two independent parameters. The sudden jump dates
418 30 March 2009, a ten of hours after the M_L 4.1 largest foreshock. . (b) A consistent trend, although
419 with much smaller time resolution, was found by *Zaccarelli et al*. [2011] for velocity variations in
420 the crust. (c) The M_L 4.1foreshock also marked a discontinuity in the seismicity rate [*Di Luccio et*
421 *al.*, 2010].
422
423 **Figure 4:** (Central panel) The grey band represents 95% of the confidence interval of FAGN/AQU
424 spectral ratio in the 1-3 Hz frequency band, and red symbols are spectral ratios of FZTW/S in the
425 same frequency band. In the small panels (a to f in chronological order), waveforms of individual

events (in red) are superimposed to the event # 1 (in black) that is used as a background reference. Panels a, b and f are relative to events with small amplitudes of trapped-waves and coherent waveforms, panels c to e are representative of waveform variations in the period between 30 March and 6 April, showing larger amplitudes and a drop of coherence. Values of CC in bold face are relative to a 4-s time window bracketing the FZTW wavetrain, and numbers in brackets are the cross-correlations of FIAM using direct body waves.

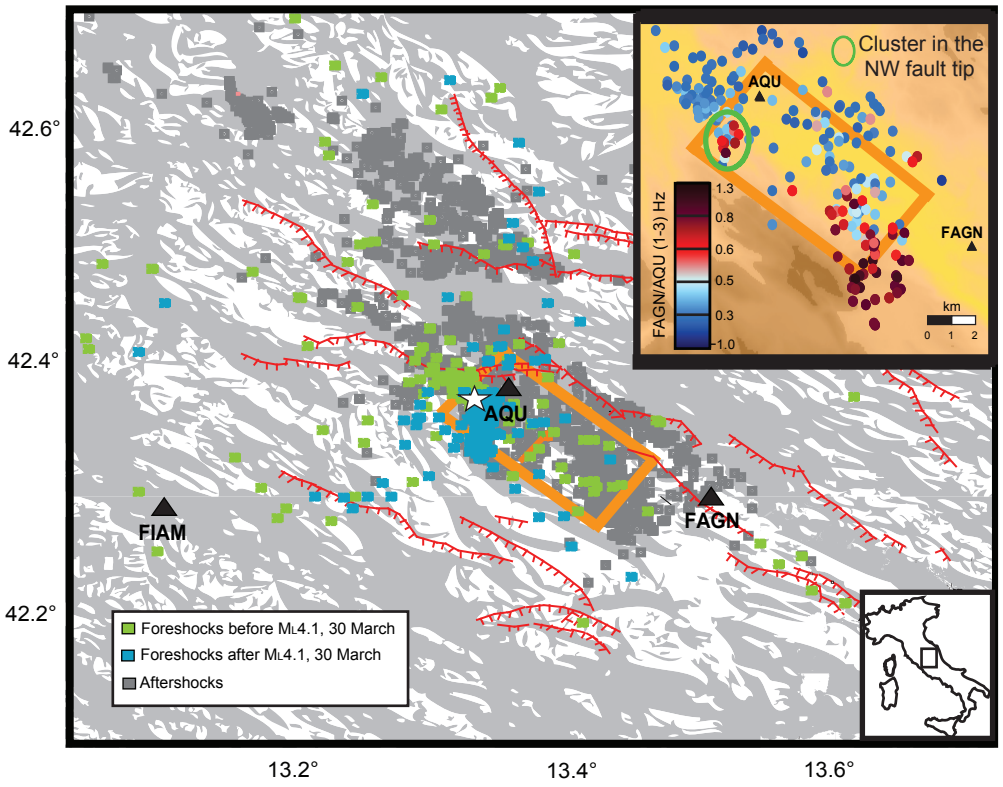
42.6°
42.4°
42.2°
13.2°
13.4°
13.6°
AQU
FIAM
FAGN
Foreshocks before ML4.1, 30 March
Foreshocks after ML4.1, 30 March
Aftershocks
Cluster in the NW fault tip
FAGN/AQU (1-3) Hz
1.3
0.8
0.6
0.5
0.3
1.0
km
0 1 2

Fig. 1

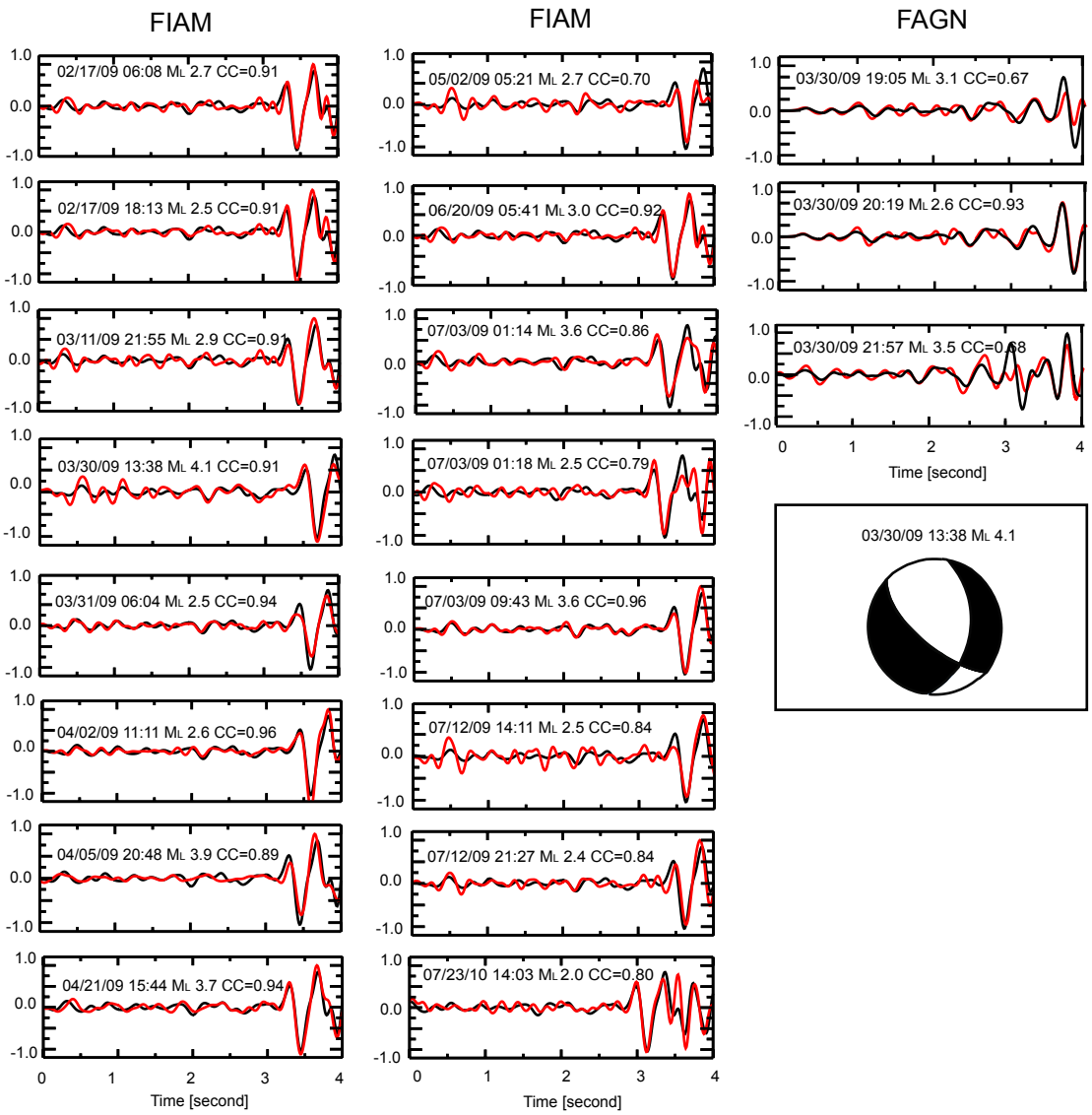
FIAM
FIAM
FAGN
02/17/09 06:08 ML 2.7 CC=0.91
02/17/09 18:13 ML 2.5 CC=0.91
03/11/09 21:55 ML 2.9 CC=0.91
03/30/09 13:38 ML 4.1 CC=0.91
03/31/09 06:04 ML 2.5 CC=0.94
04/02/09 11:11 ML 2.6 CC=0.96
04/05/09 20:48 ML 3.9 CC=0.89
04/21/09 15:44 ML 3.7 CC=0.94
05/02/09 05:21 ML 2.7 CC=0.70
06/20/09 05:41 ML 3.0 CC=0.92
07/03/09 01:14 ML 3.6 CC=0.86
07/03/09 01:18 ML 2.5 CC=0.79
07/03/09 09:43 ML 3.6 CC=0.96
07/12/09 14:11 ML 2.5 CC=0.84
07/12/09 21:27 ML 2.4 CC=0.84
07/23/10 14:03 ML 2.0 CC=0.80
03/30/09 19:05 ML 3.1 CC=0.67
03/30/09 20:19 ML 2.6 CC=0.93
03/30/09 21:57 ML 3.5 CC=0.88
1.0
0.0
-1.0
0
1
2
3
4
Time [second]
03/30/09 13:38 ML 4.1

Fig. 2

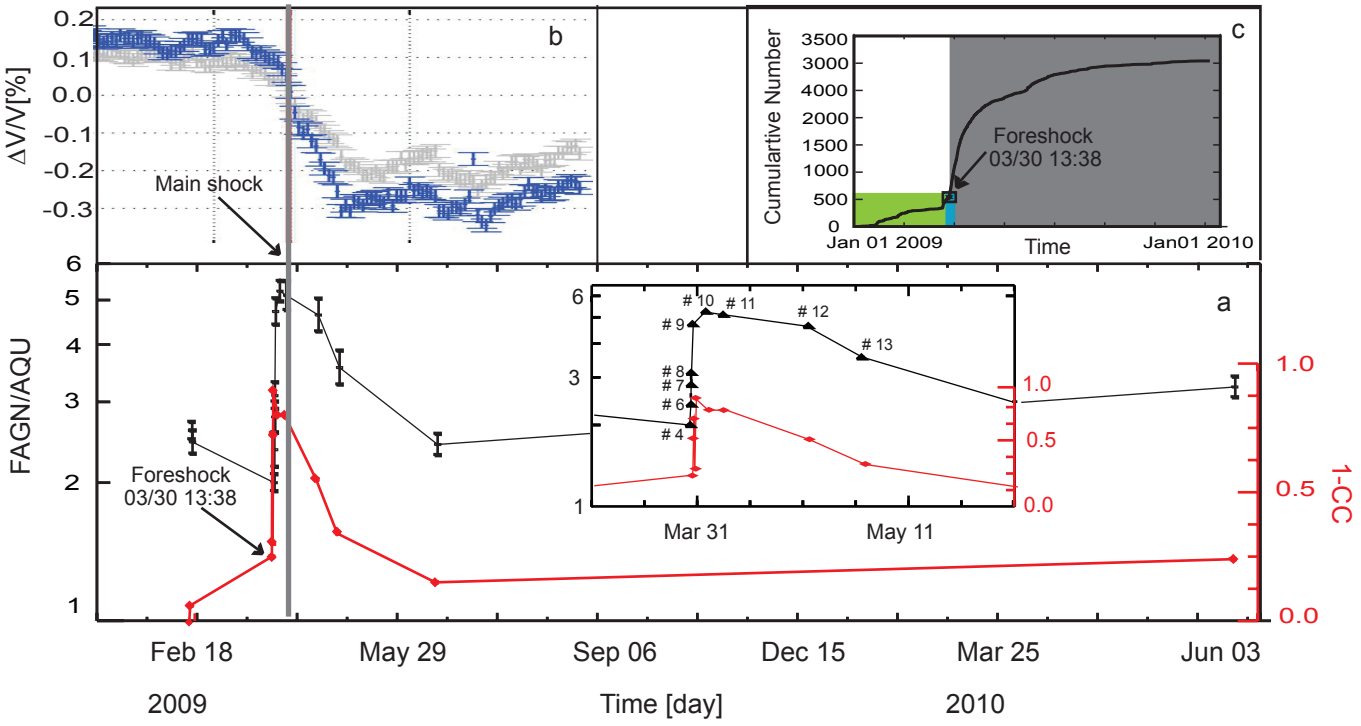
b
Main shock
ΔV/V[%]
c
Cumulative Number
Foreshock
03/30 13:38
Jan 01 2009
Time
Jan01 2010
a
FAGN/AQU
Foreshock
03/30 13:38
4
6
7
8
9
10
11
12
13
Mar 31
May 11
1-CC
Feb 18
2009
May 29
Sep 06
Time [day]
Dec 15
Mar 25
2010
Jun 03

Fig. 3

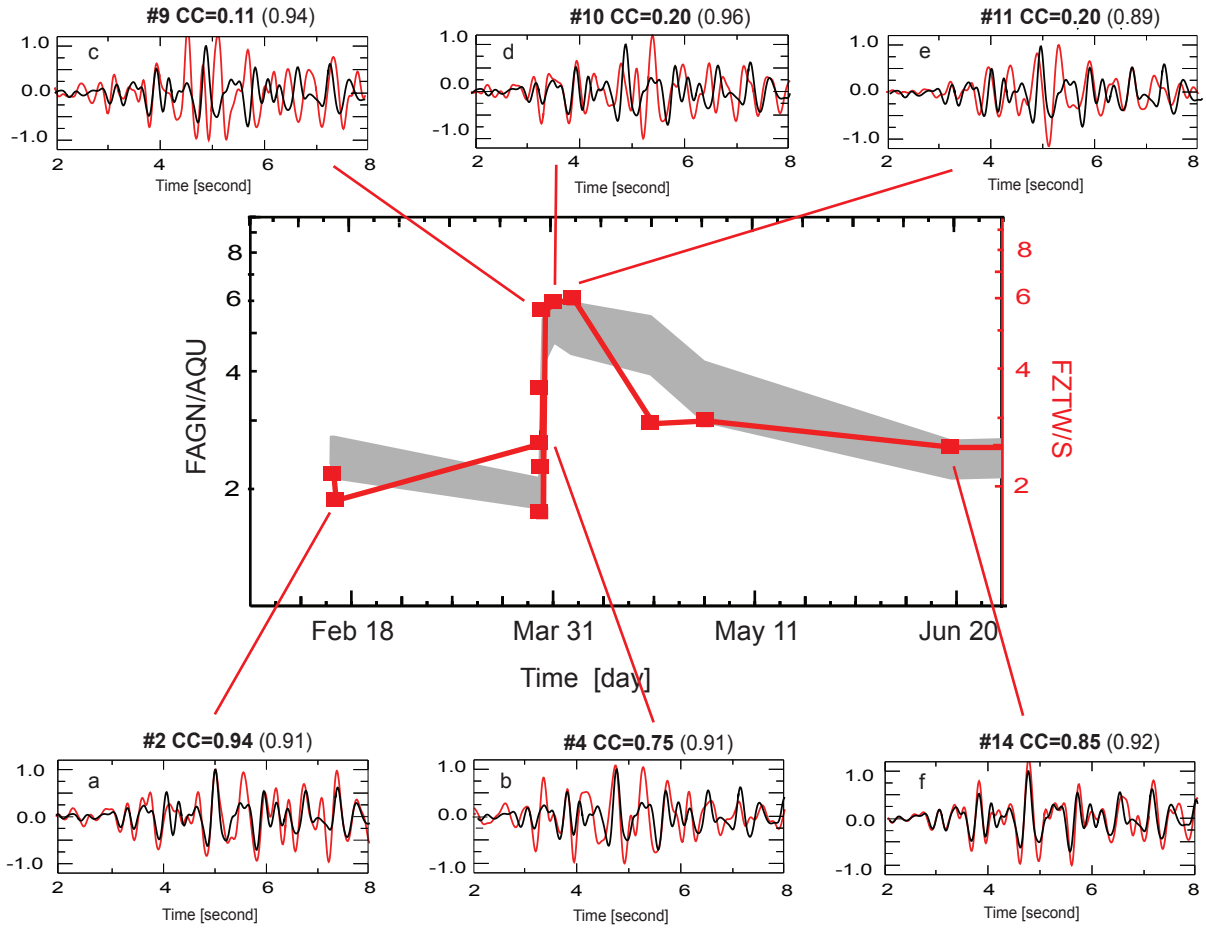
#9 CC=0.11 (0.94)
#10 CC=0.20 (0.96)
#11 CC=0.20 (0.89)
#2 CC=0.94 (0.91)
#4 CC=0.75 (0.91)
#14 CC=0.85 (0.92)
a
b
c
d
e
f
Time [second]
FAGN/AQU
FZTWS
Feb 18
Mar 31
May 11
Jun 20
Time [day]

Fig. 4

Table 1

N	Time UTC	Latitude (°)	Longitude (°)	Depth (km)	M_L	FIAM	FAGN	AQU
1	2009/02/17 06:08	42.335	13.374	9.7	2.7	X	X	X
2	2009/02/17 18:13	42.333	13.380	10.2	2.5	X	X	X
3	2009/03/11 21:55	42.325	13.383	9.4	2.9	X		X
4	2009/03/30 13:38	42.337	13.378	11.0	4.1	X	X	X
5	2009/03/30 13:43	42.315	13.378	9.7	3.4	X		
6	2009/03/30 19:05	42.316	13.373	9.7	3.1		X	X
7	2009/03/30 20:19	42.332	13.377	10.7	2.6		X	X
8	2009/03/30 21:57	42.316	13.375	9.5	3.5		X	X
9	2009/03/31 06:04	42.327	13.372	11.5	2.5	X	X	X
10	2009/04/02 11:11	42.327	13.381	10.9	2.6	X	X	X
11	2009/04/05 20:48	42.337	13.380	10.5	3.9	X	X	X
12	2009/04/21 15:44	42.324	13.371	10.0	3.7	X	X	X
13	2009/05/02 05:21	42.334	13.380	10.3	2.7	X	X	X
14	2009/06/20 05:41	42.324	13.371	9.7	3.0	X	X	X
15	2009/07/03 01:14	42.319	13.366	11.1	3.6	X		X
16	2009/07/03 01:18	42.319	13.366	10.6	2.5	X		
17	2009/07/03 09:43	42.323	13.375	10.3	3.6	X		X
18	2009/07/12 14:11	42.325	13.383	9.7	2.5	X		X
19	2009/07/12 21:27	42.329	13.372	10.4	2.4	X		X
20	2010/07/23 14:03	42.318	13.372	11.4	2.0	X	X	X